TABLE 4 Comparisons of Effective Fitting Errors (Conventional Dambrine's Method [1, 4–6]: $\bar{\varepsilon}_O$, Crupi's Method [3]: $\bar{\varepsilon}_C$, Gao's Method [2]: $\bar{\varepsilon}_G$, Proposed Method with No Optimization: $\bar{\varepsilon}_N$, and Proposed Method with Optimization: $\bar{\varepsilon}_P$)

Freq. range (GHz)	$\bar{\varepsilon}_O$ (%)	$\bar{\varepsilon}_C$ (%)	$\bar{\varepsilon}_G$ (%)	$\bar{\varepsilon}_N$ (%)	$\bar{\varepsilon}_P$ (%)
0.5–65	7.20	10.79	8.23	8.38	7.42
65.5–110	27.69	26.01	27.92	18.29	18.34
0.5–110	14.36	16.21	15.11	11.22	10.69

parameter prediction with an effective fitting error of $\bar{\varepsilon}_P = 10.69\%$.

4. CONCLUSION

From the proposed small-signal model based on the CPW de-embedded submodel method, reliable parasitic parameter sets were successfully extracted at various effective gate widths (20–140 μm) of the 0.1-μm MHEMTs in our frequency range of 0.5–110 GHz. This extraction method gave the best extraction accuracy in terms of the *S*-parameter prediction among the models reported to date with a $\bar{\varepsilon}_N$ of 11.22% without optimization and a further enhanced $\bar{\varepsilon}_P$ of 10.69% when the R_{ch} optimization scheme was used.

ACKNOWLEDGMENT

This work was supported by Dongguk University and the Basic science research program (contract number 2012001298) through the National Research Foundation of Korea (NRF) funded by the Ministry of Education.

REFERENCES

1. G. Dambrine, A. Cappy, F. Heliodore, and E. Playez, A new method for determining the FET small-signal equivalent circuit, IEEE Trans Microwave Theory Tech 36 (1988), 1151–1159.
2. J. Gao, FET small signal modeling and parameter extraction, RF and microwave modeling and measurement techniques for compound field effect transistors, SciTech Publishing, Raleigh, NC, 2010.
3. G. Crupi, D.M.M.P. Schreurs, A. Raffo, A. Caddemi, and G. Vannini, A new millimeter-wave small-signal modeling approach for pHEMTs accounting for the output conductance time delay, IEEE Trans Microwave Theory Tech 56 (2008), 741–746.
4. R. Tayrani, J.E. Gerber, T. Daniel, R.S. Pengelly, and U.L. Rhode, A new and reliable direct parasitic extraction method for mesfets and HEMTs, In: Proceedings of the 23rd European Microwave Conference, Madrid, 1993, pp. 451–453.
5. J. Lu, Y. Wang, L. Ma, and Z. Yu, A new small-signal modeling and extraction method in AlGaN/GaN HEMTs, Solid State Electron 52 (2008), 115–120.
6. R.G. Brady, C.H. Oxley, and T.J. Brazil, An improved small-signal parameter-extraction algorithm for GaN HEMT devices, IEEE Trans Microwave Theory Tech 56 (2008), 1535–1544.
7. C.-H. Kim. K.-S. Yoon, J.-W. Yang, J.-H. Lee, C.-S. Park, J.-J. Lee, and K.-E. Pyun, A new extraction method to determine bias-dependent source series resistance in GaAs FET's, IEEE Trans Microwave Theory Tech 46 (1998), 1242–1250.
8. G. Kompa, Reliable extraction of small-signal elements of a generalized distributed FET model, In: IEEE MTT-S International Microwave Symposium Digest, Vol. 1, Baltimore, MD, June 1998, pp. 291–294.
9. A. Caddemi, G. Crupi, and A. Macchiarella, On wafer-scaled GaAs HEMTs: Direct and robust small signal modeling up to 50 GHz, Microwave Opt Technol Lett 51 (2009), 1958–1963.
10. S.-W. Moon, B.-C. Jun, S.-H. Jung, D.-S. Park, J.-K. Rhee, and S.-D. Kim, Small-signal modeling approach to 0.1-μm metamorphic HEMTs for W-band coplanar MMIC amplifier design, Curr Appl Phys 12 (2012), 81–88.
11. S.-W. Moon, J.-H. Oh, Y.-H. Baek, M. Han, J.-K. Rhee, and S.-D. Kim, Millimeter-wave small-signal modeling with optimizing sensitive-parameters for metamorphic high electron mobility transistors, IOP Sci Technol 25 (2010), 063001.
12. T.T.-L. Nguyen and S.-D. Kim, Millimeter-wave small signal model using a coplanar waveguide de-embedded sub-model for HEMT, IEEE Microwave Wireless Compon Lett 24 (2013), 99–101.
13. T.T.-L. Nguyen and S.-D. Kim, A gate-width scalable method of parasitic parameter determination for distributed HEMT small-signal equivalent circuit, IEEE Trans Microwave Theory Tech 61 (2013), 3632–3638.
14. A. Jarndal and G. Kompa, A new small-signal modeling approach applied to GaN devices, IEEE Trans Microwave Theory Tech 53 (2005), 3440–3448.

WIDEBAND IMPEDANCE TRANSFORMER WITH OUT-OF-BAND SUPPRESSION CHARACTERISTICS

Phirun Kim, Girdhari Chaudhary, and Yongchae Jeong
Division of Electronics and Information Engineering, IT convergence Research Center, Chonbuk National University, Jeonju, Republic of Korea; Corresponding author: ycjeong@jbnu.ac.kr

Received 18 March 2014

ABSTRACT: *This article presents the design of a wideband impedance transformer with out-of-band suppression characteristics. The out-of-band suppression characteristics are obtained by loading several transmission zeros at both the lower and upper stop-bands. For experimental validation, a 50-to-25 Ω transformer has been implemented at a center frequency (f_0) of 2.6 GHz. The measured results were in good agreement with simulations, showing a return loss better than 20 dB over 0.92 GHz (2.1–3.02 GHz) and an out-of-band suppression better than 18 dB over DC to 1.42 and 3.8 to 6.65 GHz.* © 2014 Wiley Periodicals, Inc. Microwave Opt Technol Lett 56:2612–2616, 2014; View this article online at wileyonlinelibrary.com. DOI 10.1002/mop.28664

Key words: *coupled line; transmission zeros; wideband impedance transformer*

1. INTRODUCTION

An impedance transformer is one of the fundamental components used in RF circuit design and is widely used in impedance matching circuits, power dividers [1], combiners, and baluns [2]. A conventional impedance transformer is a quarter-wavelength transmission line (TL) [3] that provides a narrow bandwidth response that only matches perfectly at the center frequency. A multiple-section quarter-wavelength TL can be used to provide a wideband impedance matching response, but these results in an increase in the physical size of the transformer [4, 5].

Parallel coupled lines have been introduced in various RF circuit designs. Some efforts have been made to design coupled line impedance transformers using various configurations. In [6], a single-section coupled line impedance transformer was introduced. As this work focused on designing perfect matching at only the center frequency, it provides a narrowband response. For wideband characteristics, a multisection coupled TL impedance transformer was introduced in [7]. Similarly, the wideband impedance transformer composed of a coupled line and a TL was presented in [8]. However, this requires a tight coupling to obtain a high impedance transforming ratio. A quarter-wavelength step impedance TL connected from the output port to the coupling port of a coupled line using an air bridge connection was presented in [9] to increase the bandwidth. Alternatively, a shunt coupled line impedance transformer with the through port of the coupled line terminated as a short-circuit and the isolation port connected back to the input port was proposed in [10]. However, these works focused on designing only wide in-band characteristics and ignored the out-of-band suppression characteristics. Out-of-band suppression characteristics are an important design issues when an impedance transformer is applied to the design of RF circuits (e.g., a high power, high efficiency, and linear power amplifier) [11, 12]. Moreover, if the in-band matching and out-of-band noise suppression characteristics can be obtained simultaneously with the wideband impedance transformer, the RF system will be compact, inexpensive, and can eliminate the band pass filter and/or relax the specifications of the filter.

In this article, the design of a wideband impedance transformer with out-of-band suppression characteristics is presented. Theoretical analysis shows that the wideband impedance transformation can be obtained by properly choosing even- and odd-mode impedances of the coupled line while the out-of-band suppression characteristics can be obtained with four transmission zeros by adding a shunt open TL at the relatively low impedance termination port between the input and output ports of the proposed structure. To verify the design procedure of the proposed wideband impedance transformer, a 50-to-25 Ω transformer was designed, simulated, and fabricated at a center frequency (f_0) of 2.6 GHz.

2. DESIGN EQUATION

Figure 1 shows the proposed structure of the wideband impedance transformer. It is composed of a parallel coupled line with open-circuited coupling and through ports and a shunt open stub TL. As shown in Figure 1, the load impedance Z_L can be transformed to the source impedance Z_s. In this structure, Z_{0e} and Z_{0o} are even- and odd-mode impedances of the coupled line. Additionally, the electrical length (θ) is a quarter-wavelength (λ/4) at the f_0. Moreover, a half-wavelength TL with characteristic impedance Z_1 is used to both enhance the operating frequency bandwidth and provide two transmission zeros at the lower and upper sides of the operating frequency band.

The reflection and transmission coefficients of the proposed structure, where a two-port network is terminated by different impedances Z_S and Z_L, are derived from the ABCD-matrices given by (1) and (2).

$$S_{11}=\frac{ArZ_S+B-CrZ_S^2-DZ_S}{ArZ_S+B+CrZ_S^2+DZ_S} \tag{1a}$$

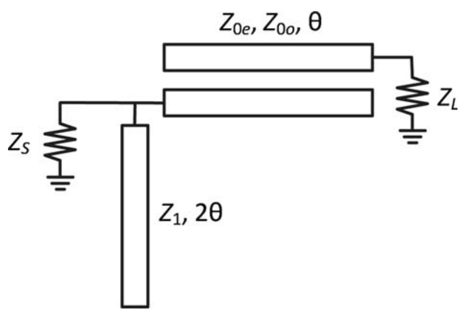

Figure 1 The proposed structure of the wideband coupled line impedance transformer

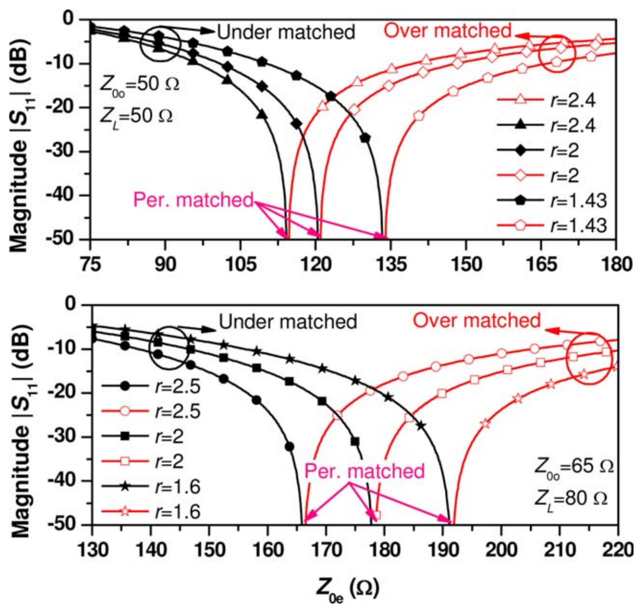

Figure 2 Return loss characteristics at the center frequency according to Z_{0e} with Z_L = 50 and 80 Ω. [Color figure can be viewed in the online issue, which is available at wileyonlinelibrary.com]

$$S_{21}=\frac{2Z_S\sqrt{r}}{ArZ_S+B+CrZ_S^2+DZ_S} \tag{1b}$$

$$A=\frac{Z_{0e}+Z_{0o}}{Z_{0e}-Z_{0o}}\cos\theta \tag{2a}$$

$$B=j\frac{(Z_{0e}+Z_{0o})^2-(Z_{0e}+Z_{0o})^2\cos^2\theta}{2(Z_{0e}-Z_{0o})\sin\theta} \tag{2b}$$

$$C=j\left[\frac{(Z_{0e}+Z_{0o})\cos\theta}{Z_1(Z_{0e}-Z_{0o})\cot(2\theta)}+\frac{2\sin\theta}{(Z_{0e}-Z_{0o})}\right] \tag{2c}$$

$$D=\frac{(Z_{0e}+Z_{0o})\cos\theta}{(Z_{0e}-Z_{0o})}-\frac{(Z_{0e}-Z_{0o})^2-(Z_{0e}+Z_{0o})^2\cos^2\theta}{2Z_1\cot(2\theta)(Z_{0e}-Z_{0o})\sin\theta} \tag{2d}$$

$$\theta=\frac{\pi f}{2f_0},\quad r=\frac{Z_L}{Z_S} \tag{2e}$$

where r and f_0 are the impedance transforming ratio and the operating center frequency, respectively.

At the f_0, the return and insertion losses can be reduced to (3a) and (3b), respectively.

$$|S_{11}|_{f=f_0}=\left|\frac{(Z_{0e}-Z_{0o})^2-4rZ_S^2}{(Z_{0e}-Z_{0o})^2+4rZ_S^2}\right| \tag{3a}$$

$$|S_{21}|_{f=f_0}=\left|\frac{4(Z_{0e}-Z_{0o})Z_S\sqrt{r}}{(Z_{0e}-Z_{0o})^2+4rZ_S^2}\right| \tag{3b}$$

As seen from (3a) and (3b), the return and insertion losses at the f_0 only depend on Z_{0e} and Z_{0o} of the coupled line and are not related with Z_1.

Figures 2(a) and 2(b) show the return loss characteristics at the f_0 according to Z_{0e} for $Z_{0o}=50$ Ω, $Z_L=50$ Ω, $Z_S=20.8$, 25, and 35 Ω (or $r=2.4$, 2, and 1.43) and $Z_{0o}=65$ Ω, $Z_L=80$ Ω, $Z_S=32$, 40, and 50 Ω (or $r=2.5$, 2, and 1.6), respectively. It is observed that there are three different regions, depending on Z_{0e}, which can be described by (4).

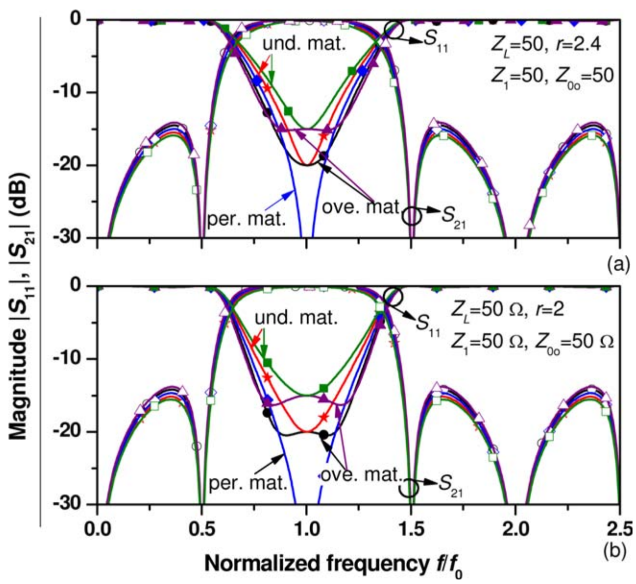

Figure 3 Simulated insertion and return losses characteristics for the specific matched conditions for return losses of 15 and 20 dB with $Z_L = 50\ \Omega$ and: (a) $r = 2.4$ and (b) $r = 2$. [Color figure can be viewed in the online issue, which is available at wileyonlinelibrary.com]

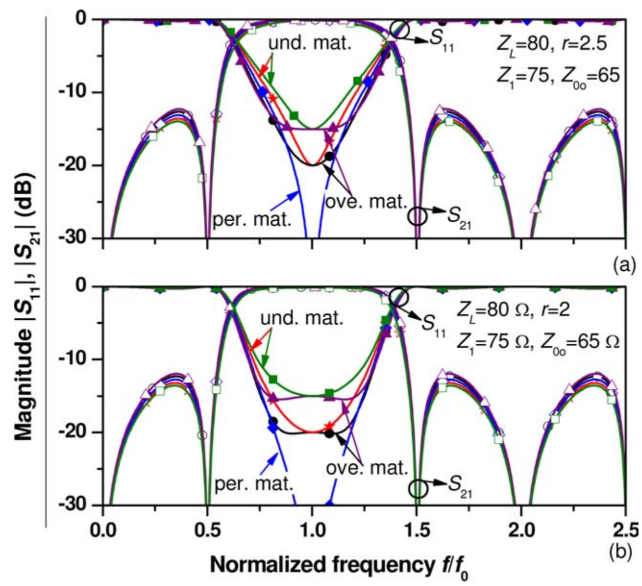

Figure 4 Simulated insertion and return losses characteristics for the specific matched conditions for return losses of 15 and 20 dB with $Z_L = 80\ \Omega$ and: (a) $r = 2.5$ and (b) $r = 2$. [Color figure can be viewed in the online issue, which is available at wileyonlinelibrary.com]

$$(Z_{0e} - Z_{0o}) < 2Z_s\sqrt{r}\quad : \text{under-matched} \tag{4a}$$

$$(Z_{0e} - Z_{0o}) = 2Z_s\sqrt{r}\quad : \text{perfectly-matched} \tag{4b}$$

$$(Z_{0e} - Z_{0o}) > 2Z_s\sqrt{r} : \text{over-matched} \tag{4c}$$

The value of Z_{0e} with specified values of S_{11}, Z_s, and r at the f_0 can be found for an under-matched case as shown by (5).

$$Z_{0e} = 2Z_S\sqrt{\frac{r\left(1-|S_{11}|_{f=f_0}\right)}{\left(1+|S_{11}|_{f=f_0}\right)}} + Z_{0o} \tag{5}$$

Similarly, the value of Z_{0e} with specified values of S_{11}, Z_s, and r at f_0 can be found for an over-matched case as shown by (6).

$$Z_{0e} = 2Z_S\sqrt{\frac{r\left(1+|S_{11}|_{f=f_0}\right)}{\left(1-|S_{11}|_{f=f_0}\right)}} + Z_{0o} \tag{6}$$

In the perfectly-matched case, S_{11} becomes zero so that the value of Z_{0e} is related with Z_s and r at the f_0 and can be found by (7).

$$Z_{0e} = 2Z_S\sqrt{r} + Z_{0o} \tag{7}$$

From (1b), the normalized transmission zeros frequencies are given by (8).

$$f_{zt}/_{f_0} = \frac{(2n-1)}{2} \tag{8a}$$

$$f_{zc}/_{f_0} = 2n \tag{8b}$$

where n, f_{zt}, and f_{zc} are integer values and the transmission zero frequencies generated by the TL and coupled line, respectively.

To verify the analysis, the insertion and return loss characteristics are shown in Figures 3 and 4 for specific return losses (15 and 20 dB) in the cases of under-, perfectly-, and over-matched conditions. Figures 3(a) and 3(b) show the simulated return losses for $Z_L = 50\ \Omega$, $Z_1 = 50\ \Omega$, $Z_{0o} = 50\ \Omega$, and $r = (2.4$ and $2)$, respectively. Additionally, Figures 4(a) and 4(b) show the simulated return losses for $Z_L = 80\ \Omega$, $Z_1 = 75\ \Omega$, $Z_{0o} = 65\ \Omega$, and $r = (2.5$ and $2)$, respectively. As seen from these figures, the bandwidth of the higher r transformer is narrower than that of the lower one. Moreover, the wide return loss bandwidth and sharp return loss slope characteristics are obtained only in the case of the over- and perfectly-matched conditions (especially in the over-matched condition). And the transmission zero frequencies can be determined by (8).

Figure 5 shows the insertion and return losses characteristics according to different values of Z_1. As Z_1 decreases, the out-of-band suppression characteristics are improved. However, the return loss bandwidth of the pass band becomes slightly deteriorated within an almost tolerable range. The trade-off between the return loss bandwidth of the operating band and the out-of-band suppression necessitates the proper selection of Z_1.

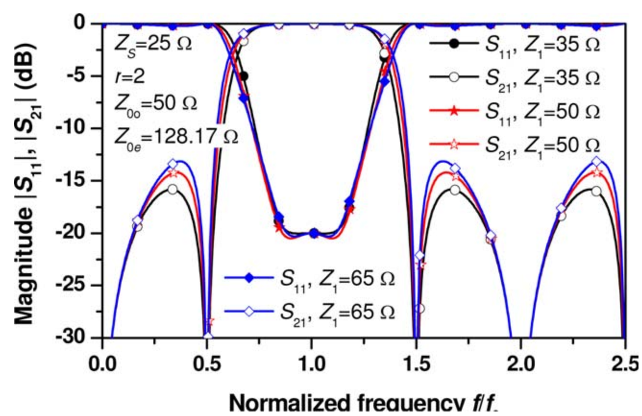

Figure 5 Simulated insertion and return losses characteristics according to different values of Z_1. [Color figure can be viewed in the online issue, which is available at wileyonlinelibrary.com]

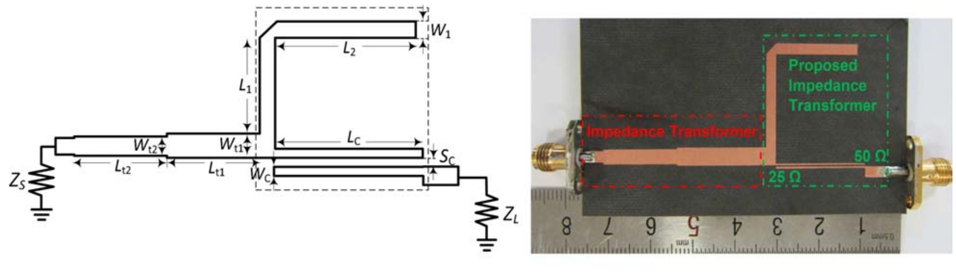

Figure 6 (a) EM simulation layout and (b) photograph of the fabricated wideband impedance transformer. [Color figure can be viewed in the online issue, which is available at wileyonlinelibrary.com]

3. SIMULATION AND MEASUREMENT RESULTS

To experimentally validate the proposed impedance transformer, a 50-to-25 Ω impedance transformer with a 20 dB return loss at 2.6 GHz was designed, simulated, and measured. According to the simulation performance shown in Figures 3 and 4, the proposed circuit can operate as a wideband impedance transformer when the circuit is operated in the over- and perfectly-matched conditions. Using (6) and selecting the Z_{0o}, it was possible to calculate Z_{0e}. Z_1 was chosen by the examining the trade-off between the return loss bandwidth of the operating band and the out-of-band suppression. The circuit was fabricated on an RT/Duroid 5880 substrate (Rogers) with a dielectric constant (ε_r) of 2.2 and a thickness (h) of 31 mils. The electromagnetic (EM) simulation was performed using HFSS v15 of Ansoft.

TABLE 1 Physical Dimension of the Proposed Wideband Impedance Transformer

$W_1 = 2.3$ mm	$L_1 = 19$ mm
$W_c = 0.31$ mm	$L_2 = 20$ mm
$S_c = 0.39$ mm	$L_c = 21$ mm
$W_{t1} = 3.8$ mm	$L_{t1} = 22.8$ mm
$W_{t2} = 3.2$ mm	$L_{t2} = 17$ mm

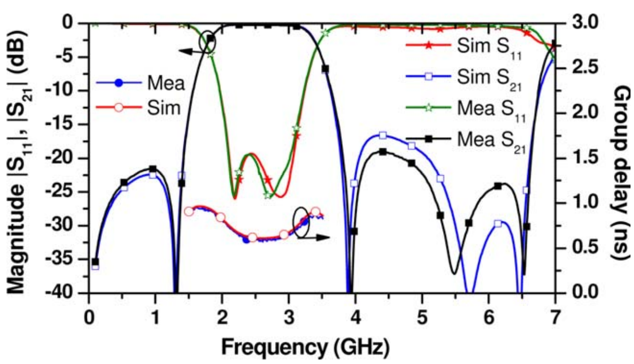

Figure 7 EM simulated and measured results of the wideband impedance transformer. [Color figure can be viewed in the online issue, which is available at wileyonlinelibrary.com]

Figure 6 shows the EM simulation layout and a photograph of the fabricated wideband impedance transformer. The two-section quarter-wavelength impedance transformer at the source port is used for the measurement with the 50 Ω termination of the network analyzer system. The circuit size of the proposed wideband impedance transformer is 28×30 mm^2 (ignoring the two-section quarter-wavelength impedance transformer). The physical dimensions of the designed impedance transformer have been slightly optimized and are shown in Table 1.

Figure 7 shows the EM simulation and measurement results for the wideband impedance transformer. The measured results are in good agreement with the simulations. From the measured results, the return loss is determined to be 22.98 dB at $f_0 = 2.6$ GHz. Similarly, the 20 dB return loss bandwidth is determined to be 0.92 GHz (2.1–3.02 GHz). The insertion loss of the impedance transformer in the pass band (2.1–3.02 GHz) is better than 0.4 dB (including the loss of the two-section quarter-wavelength impedance transformer). One transmission zero at the lower side of the operating band and three transmission zeros at the higher side of the operating band are obtained, providing selective operating band characteristics. The half-wavelength TL generates several transmission zeros: two transmission zeros are near the operating band (1.3 and 3.9 GHz) and another is at 6.53 GHz. Moreover, the quarter-wavelength coupled line generates a transmission zero at 5.48 GHz. The out-of-band signal suppression characteristic at the lower side of the operating band is more than 20 dB from DC to 1.42 GHz. Similarly, the out-of-band signal suppression characteristic at the higher side of the operating band is more than 18 dB from 3.8 to 6.65 GHz. The group delay variation in the operating band is within ±0.4 ns. Table 2 compares the performance of the proposed wideband impedance transformer with some previous studies. The 20 dB return loss bandwidth of the proposed structure is better than all of the previous impedance transformers except for [8], and the out-of-band suppression

TABLE 2 Performance Comparison of the Proposed Wideband Impedance Transformer with Previous Studies

Ref.	f_0 (GHz)	($S_{11} = -20$ dB) FBW (%)	Impedance Ratio	Out-of-Band Suppression	Structure	PCB Technology
[6]	2	≈8.5	2	NA	1-section coupled line	Microstrip line
[7]	1	≈30	2	NA	1-section coupled line	Microstrip line
[8]	1.1	≈101	2.2	NA	1-section coupled line	Strip line
This work	2.6	35.38	2	>18 dB DC to 1.42 and 3.8 to 6.65 GHz	1-section coupled line	Microstrip line

characteristics of the proposed structure are better than any of the previous circuits. Therefore, the proposed impedance transformer provides a wide operation band as well as wide out-of-band suppression characteristics. The out-of-band suppression characteristics of the proposed structure are beneficial when the circuit is used in high power, high efficiency, and wideband power amplifier designs.

4. CONCLUSION

This letter presents the design of an impedance transformer with a wide operation band as well as wide out-of-band suppression characteristics by controlling the characteristic impedances of the coupled line and the half-wavelength TL. Both theoretical and experimental measurement results are provided to validate the proposed structure. The proposed structure is simple to design and fabricate and is also expected to be applicable in various types of RF circuits and systems.

ACKNOWLEDGMENT

This work was supported by Ministry Of Trade, Industry and Energy (MOTIE) and IDEC Platform Center (IPC).

REFERENCES

1. H. Ahn and I. Wolff, General design equations, small-sized impedance transformers, and their application to small-sized three-port 3-dB power divider, IEEE Trans Microwave Theory Tech 49 (2001), 1277–1288.
2. J. Shao, R. Zhou, C. Chen, X. Wang, H. Kim, and H. Zhang, Design of a wideband balun using parallel strips, IEEE Microwave Wireless Compon Lett 23 (2013), 125–127.
3. C. Monzon, Analytical derivation of a two-section impedance transformer for a frequency and its first harmonic, IEEE Microwave Wireless Compon Lett 12 (2002), 381–382.
4. C. Marins and L. Beraldo, New design technique of N (λ/4) sections impedance transformer using geometric interpolation, In: Proceedings of IEEE International Microwave Optoelectronic Conference, 2007, pp. 127–130.
5. V. Zhurbenko, K. Kim, and K. Narenda, A compact broadband non-synchronous noncommensurate impedance transformer, Microwave Opt Technol Lett 54 (2012), 1832–1835.
6. H. Ahn and T. Itoh, Impedance-transforming symmetric and asymmetric DC blocks, IEEE Trans Microwave Theory Tech 58 (2010), 2463–2474.
7. J. Chramiec and M. Kitlinski, Design of quarter-wave compact impedance transformers using coupled transmission lines, Electron Lett 38 (2002), 1683–1685.
8. K. Ang, C. Lee, and Y. Leong, A broad-band quarter-wavelength impedance transformer with three reflection zeros within passband, IEEE Trans Microwave Theory Tech 52 (2004), 2640–2644.
9. T. Jensen, V. Zhurbenko, V. Krozer, and P. Meincke, Coupled transmission lines as impedance transformer, IEEE Trans Microwave Theory Tech 55 (2007), 2957–2965.
10. M. Chen, T. Hou, and C. Tang, Design of planar complex impedance transformers with the modified coupled line, IEEE Trans Compon Packaging Manuf Technol 2 (2012), 1704–1710.
11. J. Zhou, K. Morris, G. Watkins, and K. Yamaguchi, High-efficiency wideband class-E PA with reduced circuit elements, Microwave Opt Technol Lett 55 (2013), 323–325.
12. F.H. Raab and D. Ruppet, Frequency-agile class-D power amplifier, In: Proceedings of 9th International Conferences on HF Radio Systems Techniques Conference, 2003, pp. 81–85.

EFFICIENT RF EXTRINSIC PARAMETERS EXTRACTION TECHNIQUE FOR FinFETS

Djabar Maafri,[1,2] Mustapha C. E. Yagoub,[3] Rachida Touhami,[2] Abdelhalim Slimane,[1] and Mohand Tahar Belaroussi[1]
[1] Centre de Développement des Technologies Avancées, Cité 20 aout 1956 Baba Hassen, Alger, Algérie; Corresponding author: dmaafri@cdta.dz
[2] Instrumentation Laboratory, Faculty of Electronic and Informatique USTHB, Algiers, Algérie
[3] EECS, University of Ottawa, 800 King Edward, Ottawa, Ontario, Canada K1N 6N5

Received 26 March 2014

ABSTRACT: *Small signal RF modeling of FinFETs is strongly dependent on the methodology used to extract transistor intrinsic and extrinsic parameters. In this article, an original extraction method is proposed for determining all FinFET extrinsic series elements values from S-parameters measurements at zero bias condition. The extracted technique is demonstrated through successful comparison between simulated and measured S-parameters over a widefrequency range.* © 2014 Wiley Periodicals, Inc. Microwave Opt Technol Lett 56:2616–2619, 2014; View this article online at wileyonlinelibrary.com. DOI 10.1002/mop.28662

Key words: *FinFET; extraction method; modeling; extrinsic parameters*

1. INTRODUCTION

Modeling and characterization of FinFET devices at high frequencies have attracted a lot of attention of many researchers [1–5]. One crucial step in this process is the accurate evaluation of the extrinsic parameters of their electrical equivalent circuit. Different characterization methods have been proposed to extract such parameters, usually combining measured and simulated data [6–9]. In this work, an original direct approach is proposed based only on simulations under zero bias conditions ($V_{gs} = V_{ds} = 0$ V). It converts *S*-parametersdata to *Z*-parameters to extract the extrinsic series circuit elements and to *Y*-parameters to extract the parasitic elements [2, 7].

2. RF EXTRACTION OF THE EXTRINSIC PARAMETERS

The traditional way to determine the extrinsic parameters is first to extract the extrinsic series resistances and build the related impedance matrix Z_e. Then, to deduce the corresponding admittance matrix Y_e from which the extrinsic capacitances can be extracted.

2.1. Extraction of the Parasitic Resistance

The parasitic resistances (R_{ge}, R_{se}, R_{de}) were extracted from a set of *S*-parameters at $V_{gs} = V_{ds} = 0$ V. Under these conditions, the transistor can be represented by the electrical equivalent

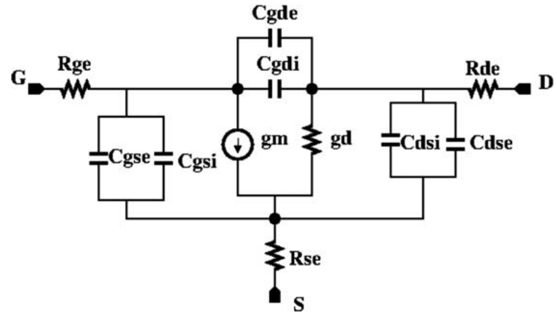

Figure 1 Small signal equivalent circuit under zero bias condition